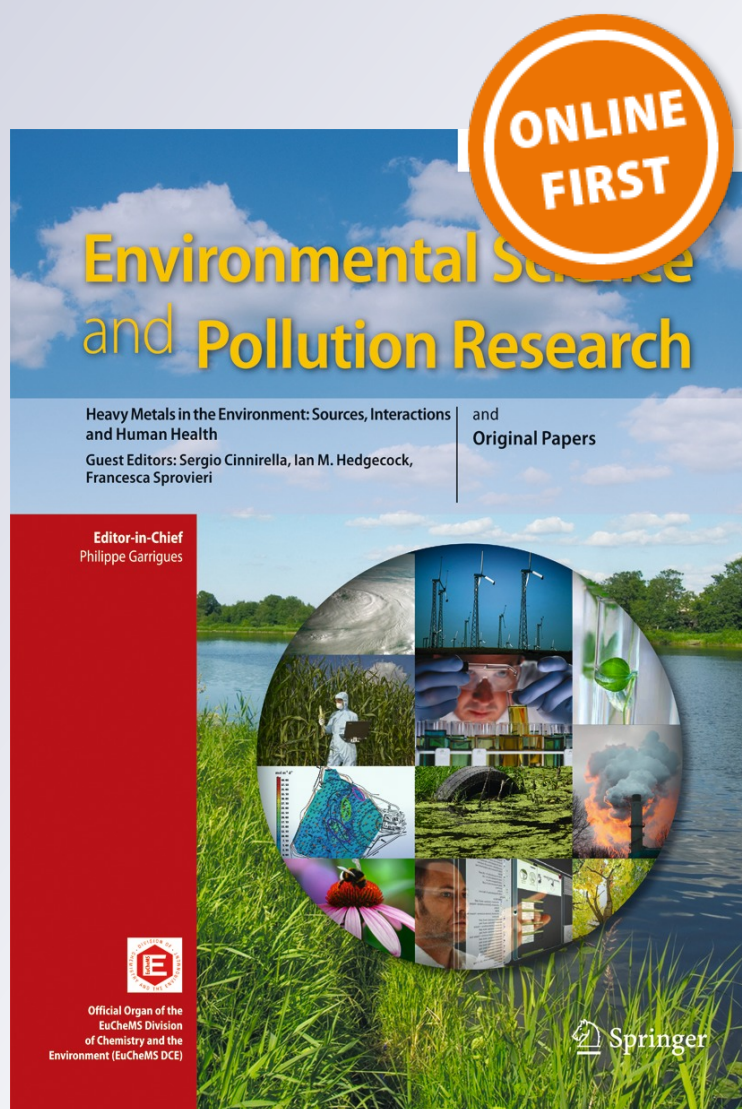# Kinetic modeling of the photocatalytic degradation of clofibric acid in a slurry reactor

Agustina Manassero, María Lucila Satuf & Orlando Mario Alfano

Environmental Science and Pollution Research

Heavy Metals in the Environment: Sources, Interactions and Human Health
Guest Editors: Sergio Cinnirella, Ian M. Hedgecock, Francesca Sprovieri

and
Original Papers

Editor-in-Chief
Philippe Garrigues

Official Organ of the
EuCheMS Division
of Chemistry and the
Environment (EuCheMS DCE)

Springer

Springer

Springer

ADVANCED OXIDATION TECHNOLOGIES: ADVANCES AND CHALLENGES IN IBEROAMERICAN COUNTRIES

Kinetic modeling of the photocatalytic degradation of clofibric acid in a slurry reactor

**Agustina Manassero · María Lucila Satuf ·
Orlando Mario Alfano**

Abstract A kinetic study of the photocatalytic degradation of the pharmaceutical clofibric acid is presented. Experiments were carried out under UV radiation employing titanium dioxide in water suspension. The main reaction intermediates were identified and quantified. Intrinsic expressions to represent the kinetics of clofibric acid and the main intermediates were derived. The modeling of the radiation field in the reactor was carried out by Monte Carlo simulation. Experimental runs were performed by varying the catalyst concentration and the incident radiation. Kinetic parameters were estimated from the experiments by applying a non-linear regression procedure. Good agreement was obtained between model predictions and experimental data, with an error of 5.9 % in the estimations of the primary pollutant concentration.

Keywords Heterogeneous photocatalysis · TiO$_2$ · Clofibric acid · Monte Carlo method · Kinetic model · UV radiation

Nomenclature

a_v	Catalytic surface area per unit suspension volume (cm^{-1})
C	Molar concentration (mol cm^{-3})
BQ	Benzoquinone
CA	Clofibric acid
4-CP	4-Chlorophenol
C_m	Catalyst mass concentration (g cm^{-3})
e^a	Local volumetric rate of photon absorption (Einstein cm^{-3} s^{-1})
e_x	Direction cosine (dimensionless)
g	Asymmetry factor (dimensionless)
l	length of flight (cm)
MC	Monte Carlo
p	Scattering phase function
q_w	Incident radiation flux (Einstein s^{-1} cm^{-2})
R_i	Random number
RMSE	Root mean square error (%)
r	Reaction rate (mol cm^{-3} s^{-1})
r_{gs}	Superficial rate of electron-hole generation (mol cm^{-2} s^{-1})
Sg	Specific surface area (cm^2 g^{-1})
t	Time (s)
V	Volume (cm^3)
x	Axial coordinate (cm)
x	Position vector (cm)

Greek letters

α_i, α_i'	Kinetic parameter
β	Volumetric extinction coefficient (cm^{-1})
ε	Hold-up (dimensionless)
η_{ph}	number of photons
ν	Stoichiometric coefficient
$\overline{\phi}$	Wavelength averaged primary quantum yield (mol Einstein^{-1})
σ	Volumetric scattering coefficient (cm^{-1})
θ	Spherical coordinate (rad)
ω	Albedo (dimensionless)

Subscripts

abs	Absorbed
A$_R$	Catalytic reaction area
BQ	Benzoquinone
CA	Clofibric acid
4-CP	4-Chlorophenol
λ	Dependence on wavelength

A. Manassero · M. L. Satuf · O. M. Alfano (✉)
Instituto de Desarrollo Tecnológico para la Industria Química,
Universidad Nacional del Litoral and Consejo Nacional de
Investigaciones Científicas y Técnicas, Güemes 3450,
Santa Fe 3000, Argentina
e-mail: alfano@intec.unl.edu.ar

HG	Henyey and Greenstein
R	Reactor
T	Total
Tk	Tank
0	Initial condition

Special symbols

< > Denotes average value over a given space

Introduction

In the last years, the presence of pharmaceuticals in drinking water and natural water systems has increased public concern because of their potential adverse effects on human health and the aquatic environment. Although the concentration of these compounds in water supplies are generally very low, their continuous input may lead to important long-term consequences in aquatic ecosystems (Wu et al. 2012).

Clofibric acid (CA) is the active metabolite of clofibrate, a pharmaceutical widely employed as blood lipid regulator. Due to its polar character, CA is not significantly adsorbed in the subsoil and it can spread easily in surface water and groundwater. CA is also resistant to biodegradation and has a very high persistence in the environment (Salgado et al. 2012).

Previous research has shown promising results in the removal of pharmaceuticals employing heterogeneous photocatalysis with titanium dioxide (TiO_2) (Giraldo et al. 2010; Martínez et al. 2011; De la Cruz et al. 2013). The photocatalytic degradation of CA has already been demonstrated, reaction intermediates have been identified, and degradation pathways have been proposed (Doll and Frimmel 2004; 2005). However, intrinsic kinetic data has not yet been published. To obtain kinetic parameters independent of the experimental conditions, the local volumetric rate of photon absorption (LVRPA) must be calculated. The most common methods to determine the LVRPA are the discrete ordinate method, the finite volume method and the Monte Carlo method (MC method) (Moreira et al. 2010). One of the main advantages of the MC method is its relatively simple application in reactors with complex configurations (Zazueta et al. 2013). Thus, it has been successfully employed to model the radiation field in different photocatalytic reactors (Changrani and Raupp 1999; Singh et al. 2007; Imoberdorf et al. 2008; Moreira et al. 2011; Zekri and Colbeau-Justin 2013; Zazueta et al. 2013; Boyjoo et al. 2013).

The present work focuses on the development of a kinetic model to represent the photocatalytic degradation of CA and the main reaction intermediates under various operating conditions. The radiation absorption in the reactor was computed by means of the MC method. Then, this information was incorporated in the kinetic model and the mass balances of the organic compounds were solved to obtain the theoretical evolution of the concentration of CA and its intermediates. Finally, the intrinsic kinetic parameters, i.e., independent of the reactor size and configuration, were estimated by applying an optimization procedure between the experimental data and those obtained with the model resolution.

The photocatalytic experiments were carried out in a slurry reactor under UV radiation and employing TiO_2 as catalyst.

Materials and methods

Chemicals

The model compound employed in the photocatalytic experiments was clofibric acid, obtained from Aldrich (CA >97 %). 4-Chlorophenol (4-CP) from Aldrich (4-CP >99 %) and benzoquinone (BQ) (BQ >98 %) from Fluka were used to identify and quantify the intermediates. The commercial TiO_2 Aeroxide P25 was employed as the photocatalyst (Evonik Degussa GmbH, Germany). All solutions were prepared with deionized and doubly distilled water.

The reactor

The photocatalytic degradation of CA was carried out in a cylindrical glass reactor with two circular flat windows. The illuminated window was made of borosilicate ground glass. A halogenated mercury lamp (150 W Powerstar HQI from OSRAM), placed at the focal axis of a parabolic reflector, was used as the light source. The lamp emits between 350 and 550 nm (UV and visible range). A container with a solution of $CoSO_4$ was interposed between the reactor and the lamp in order to block visible light. The resulting radiation that arrives at the reactor window was comprised between 350 and 420 nm. Optical neutral filters were used to carry out experiments at different irradiation levels: 100, 62, and 30 %. Figure 1 presents the spectral distribution of radiation at the reactor window and the UV-Vis absorption spectrum of CA. As can be observed in the figure, CA does not absorb radiation above 280 nm.

The reactor was operated in a closed recirculating circuit driven by a peristaltic pump (Masterflex, flow rate 1.5 L min^{-1}). The system was completed with a storage tank equipped with a water-circulating jacket to ensure isothermal conditions during the experiments (20 °C). The tank contained a device for withdrawal of samples, a thermometer, and a gas inlet for oxygen supply. Figure 2 shows a schematic representation of the experimental setup and Table 1 presents the main characteristics of the system.
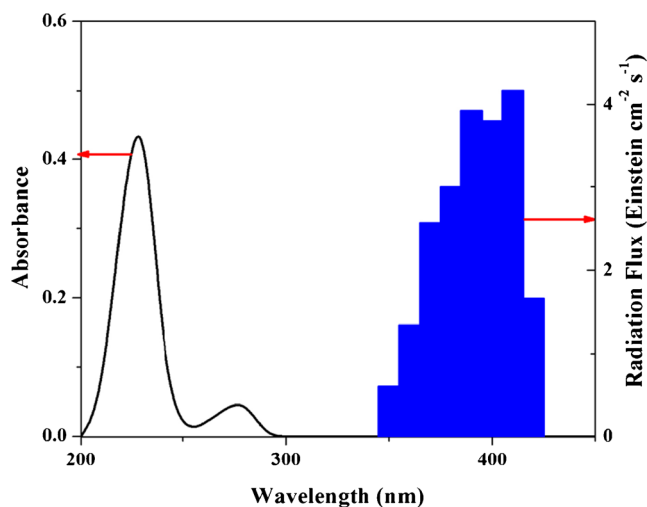
Fig. 1 Spectral distribution of radiation at the reactor window and the UV-Vis absorption spectrum of CA

Experimental procedure

For each experiment, the suspension was prepared by adding a defined mass of CA and TiO$_2$ Aeroxide P25 to a 1,000-mL volumetric flask, diluting to volume with ultrapure water and then sonicating for 30 min. The reacting mixture was added to the tank and circulated in the reactor for 60 min to achieve the adsorption equilibrium between CA and the catalyst. During this time, the suspension was saturated with pure oxygen by intense bubbling and the lamp was turned on to stabilize the radiation emission. To prevent the arrival of radiation at the reactor, a shutter was placed between the lamp and the reactor window. When the system was stabilized and adsorption equilibrium was reached, the first sample was taken ($t=0$) and then the shutter was removed. Throughout the reaction, the system was maintained under overpressure of oxygen to guarantee the renewal of the oxygen consumed. Each experiment lasted 360 min and sampling was done every 60 min. TiO$_2$ suspension samples were separated out by centrifugation

and filtered through a 0.02 μm (Anotop 25) to remove the catalyst particles before analysis.

The incident radiation fluxes at the reactor window under different irradiation levels were experimentally measured by ferrioxalate actinometry (Murov et al. 1993).

In order to calibrate the kinetic model, experiments were carried out under different operating conditions, as detailed in Table 2.

Analysis

The concentration of CA and its primary intermediates (4-CP and BQ) were measured by HPLC with a UV detector using a Waters chromatograph provided with a RP C-18 column (XTerra®). The mobile phase was a binary mixture of acidified water (with 0.1 %v/v phosphoric acid) and acetonitrile (50:50). The flow rate was 1.0 mL min^{-1} and the injection volume was 20 μL (Dordio et al. 2009). Absorbance detection was made at 227 nm for CA and 4-CP and at 254 nm for BQ.

Mass balances

In order to obtain the theoretical evolution of the concentration of CA and the main intermediates, it is necessary to solve the mass balance for each species. Assuming that: (i) the conversion per pass in the reactor is differential, (ii) the system is well-mixed, (iii) there are no mass transport limitations, (iv) the chemical reactions occurs only at the solid-liquid interface, and (v) direct photolysis is neglected, the mass balance for the species i results (Satuf et al. 2007):

$$\left.\varepsilon_L \frac{dC_i(t)}{dt}\right|_{Tk} = \frac{V_R}{V_T} a_v v_i \langle r(\boldsymbol{x},t)\rangle_{A_R} \tag{1}$$

where ε_L is the liquid hold-up ($\varepsilon_L \cong 1$), C_i is the molar concentration of i, t denotes reaction time, Tk refers to the tank, v_i is

Fig. 2 Schematic representation of the experimental setup: (*1*) filter, (*2*) reactor, (*3*) lamp and reflector, (*4*) pump, (*5*) tank, (*6*) thermometer, (*7*) oxygen and (*8*) thermostatic bath
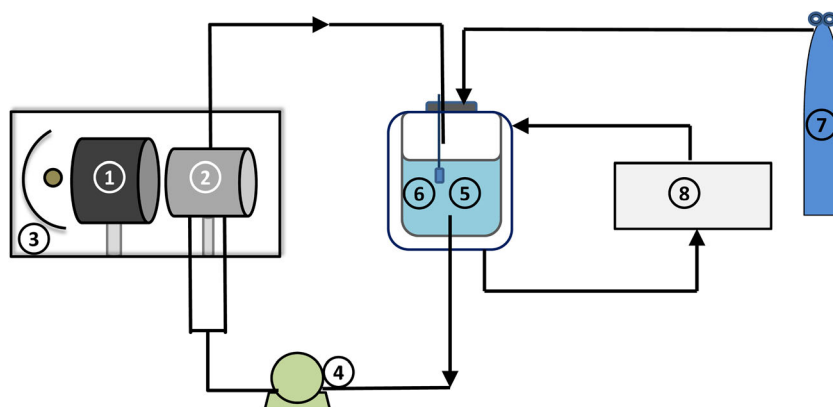
Table 1 Main characteristics of the system

Component	Parameter	Value
Reactor	Inner diameter	5.0 cm
	Length	2.75 cm
	Volume (V_R)	54 cm^3
	Suspension volume (V_T)	1,000 cm^3
Lamp	Nominal power	150 W
	Length	132 mm
	Diameter	23 mm
	UV radiation flux (100 %)	1.52×10^{-8} (Einstein s^{-1} cm^{-2})
	UV radiation flux (62 %)	9.39×10^{-9} (Einstein s^{-1} cm^{-2})
	UV radiation flux (30 %)	4.58×10^{-9} (Einstein s^{-1} cm^{-2})

the stoichiometric coefficient, a_v denotes the catalytic surface area per unit suspension volume, $\langle r(\mathbf{x},t) \rangle_{A_R}$ is the superficial reaction rate averaged over the catalytic reaction area A_R, and V_R and V_T are the reactor and the total system volumes, respectively. The value of a_v is computed from the product of the catalyst specific surface area (Sg) and the catalyst loading (C_m).

A simplified reaction pathway for the photocatalytic degradation of CA is proposed in Fig. 3 (Doll and Frimmel 2004). Based on this scheme, the mass balances for CA and the intermediates 4-CP and BQ, with the respective boundary conditions, can be expressed as:

$$\varepsilon_L \frac{dC_{CA}(t)}{dt}\bigg|_{Tk} = -\frac{V_R}{V_T} a_v \left\{ \langle r_{CA,1}(\mathbf{x},t) \rangle_{A_R} + \langle r_{CA,2}(\mathbf{x},t) \rangle_{A_R} \right\} \quad (2)$$
$$C_{CA}(t=0) = C_{CA,0}$$

$$\varepsilon_L \frac{dC_{4-CP}(t)}{dt}\bigg|_{Tk} = \frac{V_R}{V_T} a_v \left\{ \langle r_{CA,1}(\mathbf{x},t) \rangle_{A_R} - \langle r_{4-CP,1}(\mathbf{x},t) \rangle_{A_R} - \langle r_{4-CP,2}(\mathbf{x},t) \rangle_{A_R} \right\}$$
$$C_{4-CP}(t=0) = 0$$
$$\quad (3)$$

$$\varepsilon_L \frac{dC_{BQ}(t)}{dt}\bigg|_{Tk} = \frac{V_R}{V_T} a_v \left\{ \langle r_{CA,2}(\mathbf{x},t) \rangle_{A_R} + \langle r_{4-CP,2}(\mathbf{x},t) \rangle_{A_R} - \langle r_{BQ}(\mathbf{x},t) \rangle_{A_R} \right\}$$
$$C_{BQ}(t=0) = 0$$
$$\quad (4)$$

Table 2 Experimental conditions

Variable	Value
Initial concentration of CA (mol cm^{-3})	9.30×10^{-8}
pH	Natural (5)
Catalyst concentration (g L^{-1})	0.1, 0.25, 0.5, and 1.0
Level of incident radiation (%)	30, 62, and 100

where $r_{CA,1}$ and $r_{CA,2}$ represent the degradation rates of CA to give the intermediate 4-CP and BQ, respectively. Furthermore, $r_{4\text{-}CP,1}$ and $r_{4\text{-}CP,2}$ refer to the rate of degradation of 4-CP to generate secondary organic intermediates and BQ, respectively. Finally, r_{BQ} represents the degradation rate of benzoquinone.

The resolution of the mass balance implies: (i) the development of a kinetic model to obtain the reaction rate expressions for CA and its intermediates, and (ii) the calculation of the LVRPA.

(i) Kinetic model:

Table 3 shows the proposed reaction scheme for the photocatalytic degradation of CA. The reaction begins when TiO$_2$ absorbs UV radiation. This promotes an electron from the valence band of the semiconductor into the conduction band, leaving a positively charged hole in the valence band. The photogenerated electron-hole pair migrates to the surface of the catalyst particle and reacts with surface species. The electrons and holes have to be trapped to prevent recombination and the resulting loss of energy as heat. Electrons can be trapped by molecular oxygen, generating the superoxide radical anion and holes can be trapped by water molecules or hydroxyl ions adsorbed at the catalyst surface, leading to the formation of hydroxyl radicals. Hydroxyl radicals can attack the CA molecule to give two primary organic intermediates: 4-CP and BQ. In turn, 4-CP can be further degraded by oxidation with hydroxyl radicals, giving BQ and other secondary organic intermediates, X_i. Also, BQ can be degraded and transformed into X_j intermediates. Y_l represents inorganic species and radicals that compete with organic molecules for hydroxyl radicals (Turchi and Ollis 1990; Almquist and Biswas 2001).

To obtain the reaction rate expressions, the following assumptions have been considered:

(i) Photocatalytic reactions occur at the surface of the catalyst particles among adsorbed species (Pelizzetti and Minero 1993).
(ii) A dynamic equilibrium is achieved between the bulk and the adsorbed concentrations of H$_2$O, O$_2$, inorganic species and organic compounds (Almquist and Biswas 2001; Dijkstra et al. 2002).
(iii) Molecular oxygen and organic compounds are adsorbed on different sites in the catalyst particle (Turchi and Ollis 1990; Terzian et al. 1990).
(iv) A mechanism of competitive adsorption between CA and its main reaction intermediates is postulated.
(v) The attack by the hydroxyl radical is the main degradation pathway for CA and its intermediates (Mills et al. 1993; Theurich et al. 1996).

Fig. 3 Reaction pathway for the CA degradation
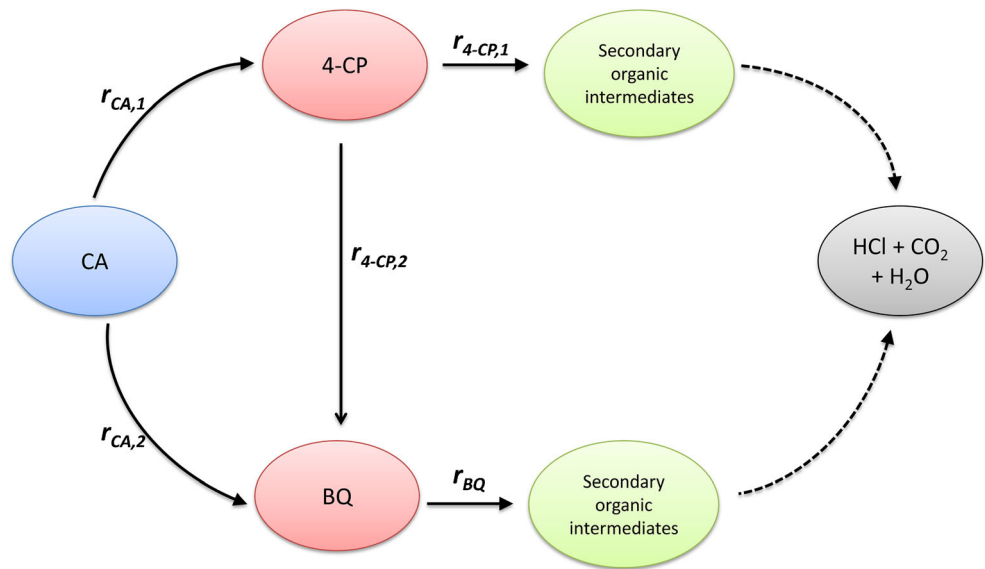
(vi) There are no limitations to the mass transport (Satuf et al. 2007).
(vii) O_2 concentration is constant and in excess with respect to the stoichiometric demand (Satuf et al. 2007).
(viii) The concentration of water molecules and hydroxyl ions on the catalytic surface remains constant (Satuf et al. 2007).
(ix) The superficial concentration of total absorption sites for CA, per unit area of catalyst, can be considered constant.

Table 3 Reaction scheme for the photocatalytic degradation of CA

Stage	Reaction	Rate
Activation	$TiO_2 + h\nu \rightarrow e^- + h^+$	r_{gs}
Recombination	$e^- + h^+ \rightarrow heat$	$k_2[e^-][h^+]$
Electron trapping	$e^- + O_{2,ads} \rightarrow \cdot O_2^-$	$k_3[e^-][O_{2,ads}]$
Hole trapping	$h^+ + H_2O_{ads} \rightarrow \cdot OH + H^+$	$k_4[h^+][H_2O_{ads}]$
	$h^+ + OH_{ads}^- \rightarrow \cdot OH$	
Hydroxyl attack	$CA_{ads} + \cdot OH \rightarrow 4\text{-}CP$	$k_5[CA_{ads}][\cdot OH]$
	$CA_{ads} + \cdot OH \rightarrow BQ$	$k_6[CA_{ads}][\cdot OH]$
	$4\text{-}CP_{ads} + \cdot OH \rightarrow X_i$	$k_7[4\text{-}CP_{ads}][\cdot OH]$
	$4\text{-}CP_{ads} + \cdot OH \rightarrow BQ$	$k_8[4\text{-}CP_{ads}][\cdot OH]$
	$BQ_{ads} + \cdot OH \rightarrow X_j$	$k_9[BQ_{ads}][\cdot OH]$
	$Y_{l,ads} + \cdot OH \rightarrow Y_m$	$k'_1[Y_{l,ads}][\cdot OH]$
Adsorption	$site_{O_2} + O_2 \leftrightarrow O_{2,ads}$	
	$site_{H_2O} + H_2O \leftrightarrow H_2O_{ads}$	
	$site_{H_2O} + H_2O \leftrightarrow OH_{ads}^- + H^+$	
	$site_{CA} + CA \leftrightarrow CA_{ads}$	
	$site_{CA} + 4\text{-}CP \leftrightarrow 4\text{-}CP_{ads}$	
	$site_{CA} + BQ \leftrightarrow BQ_{ads}$	
	$site_{Y_l} + Y_l \leftrightarrow Y_{l,ads}$	

(x) The rate of electron-hole generation is defined as:

$$r_{gs}(x) = \frac{\overline{\phi}}{a_v} \int_\lambda e_\lambda^a(x) d\lambda$$, where $\overline{\phi}$ is the primary quantum yield averaged over the wavelength range (Alfano et al. 1997).

Taking into account all the above considerations, the following reaction rate expressions were obtained:

$$r_{CA}(x,t) = \frac{(\alpha_{2,1} + \alpha_{2,2})C_{CA}(x,t)}{1 + \alpha_3 C_{CA}(x,t) + \alpha'_1 C_{4-CP}(x,t) + \alpha'_2 C_{BQ}(x,t)} \quad (5)$$

$$\times \left(-1 + \sqrt{1 + \frac{\alpha_1}{a_v}e^a(x)}\right) \quad (6)$$

$$r_{4-CP}(x,t) = \frac{(\alpha_{4,1} + \alpha_{4,2})C_{4-CP}(x,t)}{1 + \alpha_3 C_{CA}(x,t) + \alpha'_1 C_{4-CP}(x,t) + \alpha'_2 C_{BQ}(x,t)}$$

$$\times \left(-1 + \sqrt{1 + \frac{\alpha_1}{a_v}e^a(x)}\right)$$

$$r_{BQ}(x,t) = \frac{\alpha_5 C_{BQ}(x,t)}{1 + \alpha_3 C_{CA}(x,t) + \alpha'_1 C_{4-CP}(x,t) + \alpha'_2 C_{BQ}(x,t)} \quad (7)$$

$$\times \left(-1 + \sqrt{1 + \frac{\alpha_1}{a_v}e^a(x,t)}\right)$$

where α_i represents the intrinsic kinetic parameters involved in the photocatalytic degradation of CA.

A detailed description of the steps followed to obtain the kinetic equations can be found in the Appendix.

(ii) LVRPA

As can be seen in Eqs. (5)–(7), the knowledge of the LVRPA is essential to model the kinetics in the system. The Monte Carlo approach was employed to compute the radiation absorbed in the photocatalytic reactor. This method use randomly generated numbers (R_i), between 0

and 1, to determine the trajectories and fates of all photons emitted by the lamp. Considering that (1) radiation extinction by the catalyst particles occurs mainly along the longitudinal axis of the cylindrical reactor, and (2) the incoming radiation at the reactor window is diffuse, photon trajectories can be described with one spatial variable (x) and one angular variable (θ). The reactor length was divided into small spatial cells to store the number of photons absorbed in each cell and subsequently calculate the LVRPA. Figure 4 shows a flowchart of the algorithm employed to calculate the LVRPA in the slurry reactor.

To build the trajectory of the photons, it is necessary to know the direction and the length of the flight, and the fate of the photon: absorption, scattering or loss (i.e., the photon hits the reactor walls or escapes through the window). Absorption and scattering phenomena depend on the photon wavelength. Therefore, the emission range of the lamp was discretized into eight wavelengths and the trajectories of photon bundles inside the reactor were traced for each wavelength using the following steps:

(1) Photon direction at the reactor window (θ). Radiation emitted from the lamp that arrives at the inner side of the reactor window is diffuse. Thus, the same probability is assigned to all the directions (Spadoni et al. 1977) and the angle θ that determines direction of the photon flight is given by:

$$\sin \theta = 2R_1 - 1 \qquad (8)$$

(2) Length of flight (l): The distance that the photon can travel in the reacting medium without interactions can be calculated by (Yokota et al. 1999):

$$l = -\frac{1}{\beta_\lambda}\ln(1 - R_2) \qquad (9)$$

where β_λ is the spectral extinction coefficient of the catalyst suspension. The new position of the photon is determined by

$$x_{\text{new}} = x_{\text{old}} + e_x l \qquad (10)$$

where x_{old} represents the previous position of the photon and e_x is the direction cosine.

(3) Fate of the photon. If the photon remains inside the reactor after traveling a distance l, it strikes a catalyst particle and two events can take place: absorption or scattering. The probability to occur one event or the other is related to the albedo: $\omega_\lambda = \sigma_\lambda/\beta_\lambda$, where σ_λ is the spectral scattering coefficient. At higher ω_λ, higher is the probability of scattering (Spadoni et al. 1977). Therefore, if

$$1 - \omega_\lambda \geq R_3 \qquad (11)$$

the photon is absorbed, stored in the corresponding cell and the trajectory ends. Otherwise, the photon is scattered and a new direction is determined by the phase function. The Henyey and Greenstein phase function ($p_{\text{HG},\lambda}$) was adopted (Siegel and Howell 2002).

Fig. 4 Flowchart of MC method
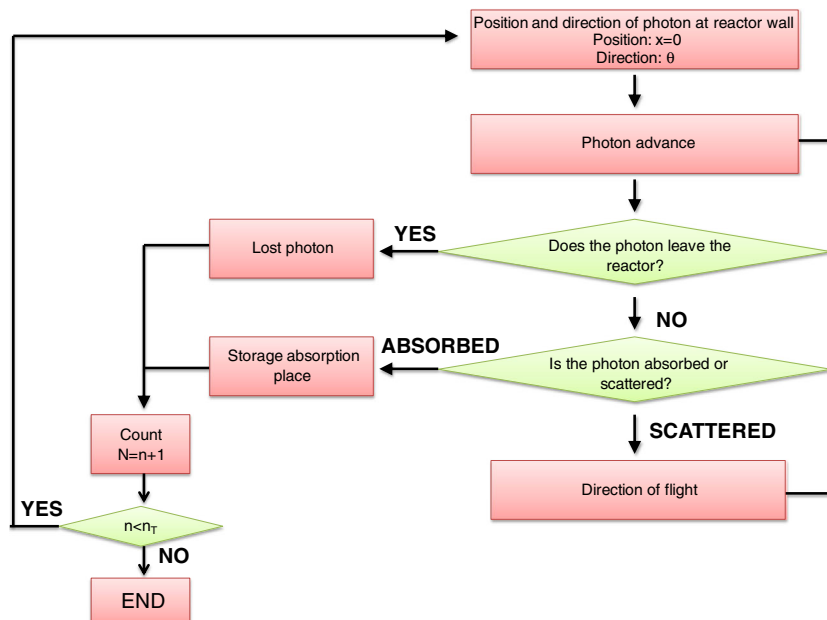
$$p_{\mathrm{HG},\lambda}(\cos\theta) = \frac{1-g_\lambda{}^2}{2\left(1+g_\lambda^2-2g_\lambda\cos\theta\right)^{3/2}} \quad (12)$$

where g_λ is the asymmetry factor. The cosine of the angle that determines the new direction of the photon is given by (Moreira et al. 2010 and Zekri and Colbeau-Justin 2013):

$$\cos\theta = \frac{1}{2g_\lambda}\left[1+g_\lambda^2-\left(\frac{1-g_\lambda{}^2}{1+g_\lambda(2R_4-1)}\right)^2\right] \quad (13)$$

Once the new direction is established, a new value of l is calculated, and the sequence of events begins again until the photon is either absorbed or lost.

The optical properties of the catalyst suspension ($\beta_\lambda, \sigma_\lambda$ and g_λ) were taken from Satuf et al. 2005.

The LVRPA in each cell of the reactor was calculated according to:

$$e^a(x) = \sum_{\lambda=350\ \mathrm{nm}}^{\lambda=420\ \mathrm{nm}} \frac{q_{w\lambda} n_{\mathrm{ph}\lambda,\mathrm{abs}}(x)}{n_{\mathrm{ph},T}\Delta x} \quad (14)$$

where $q_{w\lambda}$ is the radiation flux of wavelength λ incident at the reactor window, $n_{\mathrm{ph}\lambda,\mathrm{abs}}$ represents the number of photons of wavelength λ absorbed in a cell of position x, $n_{\mathrm{ph},T}$ is the total number of the photons considered in the simulation, and Δx is the length of the cell. The value of $q_{w\lambda}$ was calculated from the spectral distribution of the radiation emitted by the lamp (given by the manufacturer) and from the polychromatic radiation flux experimentally measured by potassium ferrioxalate actinometry (Murov et al. 1993).
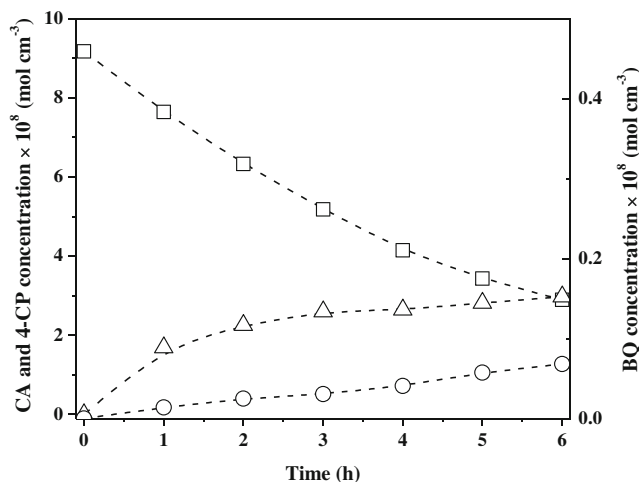

Fig. 6 LVRPA profiles for different catalyst concentrations. 0.1 g L^{-1} (*short dot line*), 0.25 g L^{-1} (*dash line*), 0.5 g L^{-1} (*dot line*), 1 g L^{-1} (*solid line*)

Results

Experimental results

Control experiments were carried out to evaluate: (i) absence of direct photolysis of CA, (ii) the time necessary to reach the adsorption equilibrium between CA and the catalyst, and, (iii) the optimum pH to perform the photacalytic runs.

These assays showed that the pollutant does not undergo photolysis because no detectable changes occurred in the CA concentration after 5 h of irradiation without catalyst. It was also determined that the adsorption equilibrium between the contaminant and TiO$_2$ was achieved after 1 h of recirculation in the reactor.

Fig. 5 Evolution of concentration of CA, 4-CP and BQ in a typical photocatalytic run (*open square*) CA; (*open upright triangle*) 4-CP; (*open circle*) BQ
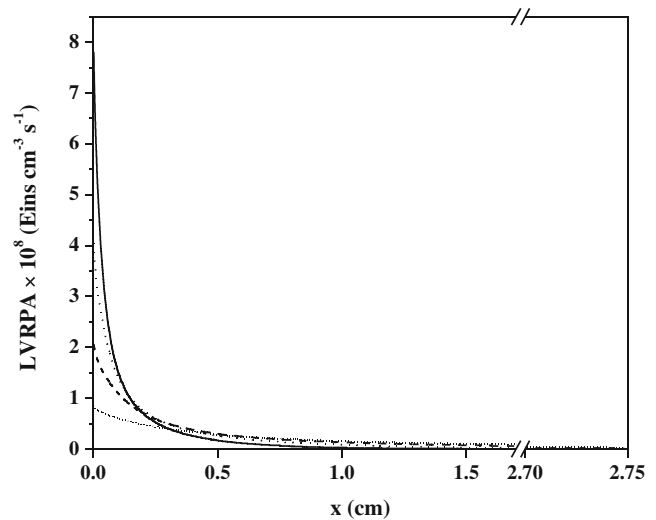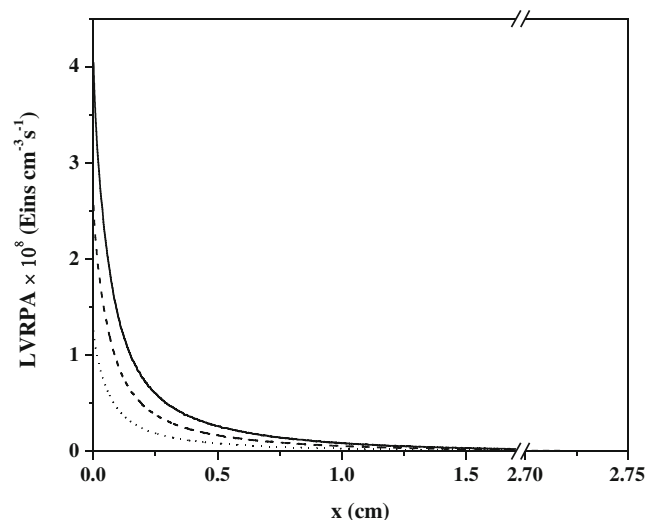

Fig. 7 LVRPA profiles for different level of irradiation and $C_m =$ 0.5 g L^{-1}. 100 % of irradiation (*solid line*), 62 % of irradiation (*dash line*), 30 % of irradiation (*dot line*)

Table 4 Estimated kinetic parameters

Parameter	Value
α_1 (s cm^2 Einstein^{-1})	6.07×10^{11}
$\alpha_{2,1}$ (cm s^{-1})	5.83×10^{-6}
$\alpha_{2,2}$ (cm s^{-1})	6.10×10^{-7}
$\alpha_{4,1}$ (cm s^{-1})	1.41×10^{-6}
$\alpha_{4,2}$ (cm s^{-1})	7.97×10^{-6}
α_5 (cm s^{-1})	4.77×10^{-4}

Furthermore, the natural pH of the suspension (pH=5) was the most favorable pH to perform the photocatalytic experiments (data not shown).

For the kinetic study, a first set of experiments was carried out by varying the catalyst concentration, with a level of irradiation of 100 %. The second set of experiments was performed with 0.5 g L^{-1} TiO$_2$ but by modifying the level of irradiation.

The reaction rates were accelerated when increasing the TiO$_2$ concentration from 0.1 to 0.5 g L^{-1}. However, there was no significant improvement when increasing the catalyst loading from 0.5 to 1.0 g L^{-1}. Thus, TiO$_2$ concentration was kept at 0.5 g L^{-1} in the second set of experiments.

Figure 5 shows the results obtained in a typical photocatalytic run (C_m=0.5 g L^{-1} and 100 % of irradiation). It can be seen that the concentration of two main aromatic intermediates (4-CP and BQ) gradually increases as CA is photocatalytically degraded. Under every experimental condition tested, the concentration of 4-CP was always higher than that of BQ.

LVRPA profiles

Figure 6 shows the LVRPA profiles obtained with Monte Carlo simulations for different catalyst concentrations. At higher TiO$_2$ loadings, the photon absorption increases near to the irradiated window of the reactor. Furthermore, as long as the TiO$_2$ concentration decreases, the LVRPA profiles are smoother. In all cases, almost all the absorbed radiation was achieved in the space comprised between the irradiated window and x=1 cm. The LVRPA profiles at different level of irradiation are shown in Fig. 7.

Estimation of the kinetic parameters

Kinetic parameters involved in Eqs. (5)–(7) were estimated by applying the Levenberg-Marquardt optimization method (Himmelblau 1970). The values of the kinetic parameters rendered by the optimization procedure are those that
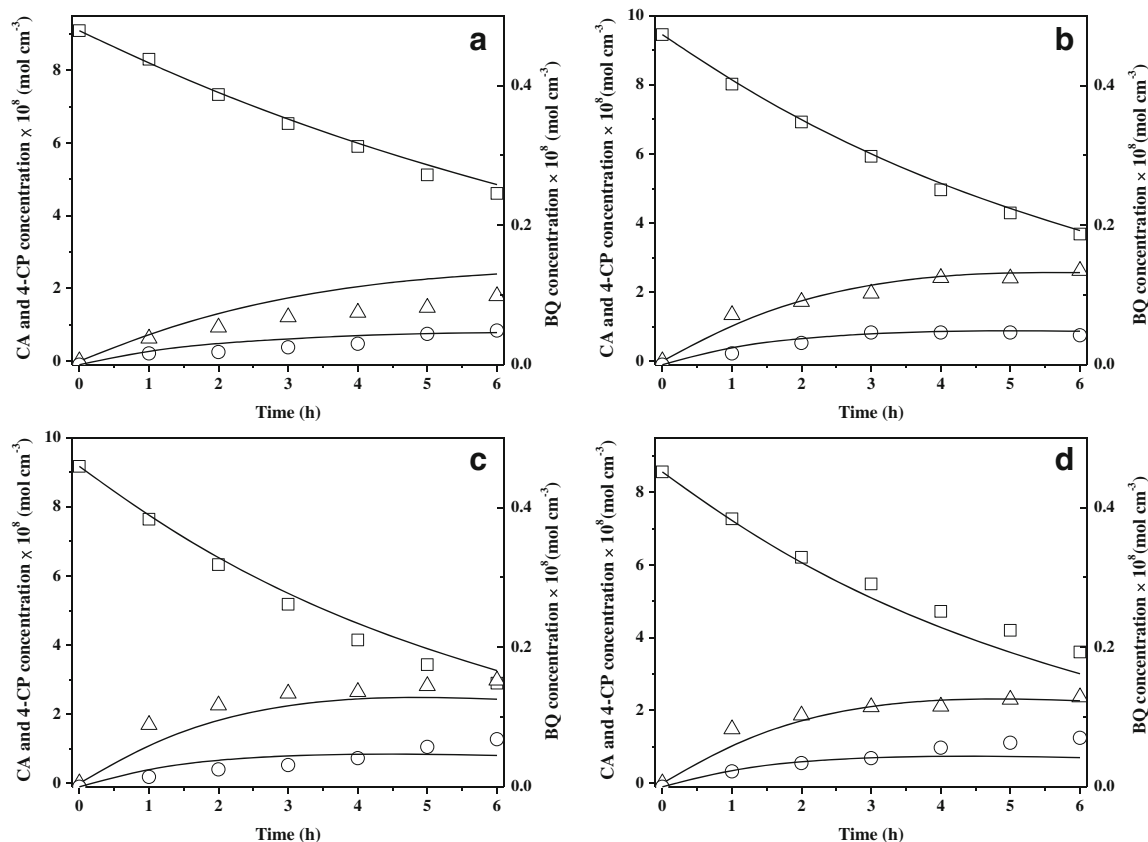

Fig. 8 Experimental and predicted concentrations of CA, 4-CP and BQ vs. time for 100 % of irradiation. Experimental data: (*open square*) CA; (*open upright triangle*) 4-CP, and (*open circle*) BQ. Model results: *solid lines*. **a** C_m=0.1 g L^{-1}; **b** C_m=0.25 g L^{-1}; **c** C_m=0.5 g L^{-1}, and **d** C_m=1 g L^{-1}
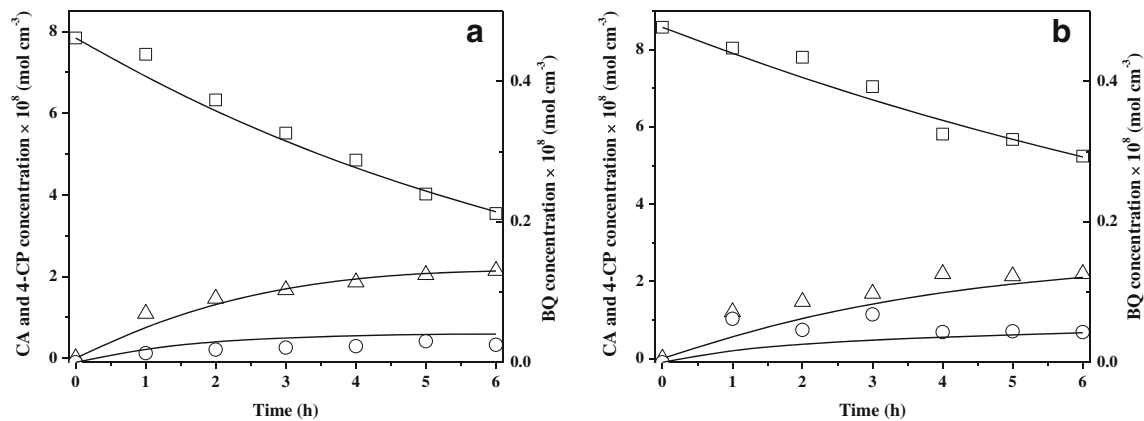
Fig. 9 Experimental and predicted concentrations of CA, 4-CP and BQ vs. time for $C_m = 0.5$ g L^{-1}. Experimental data: (*open square*) CA; (*open upright triangle*) 4-CP and (*open circle*) BQ. Model results: *solid lines*. **a** Level of irradiation=62 %; **b** level of irradiation=30 %

minimize the differences between the experimental concentrations of CA, 4-CP and BQ, and the corresponding concentrations predicted by the model. The terms $\alpha_3 C_{CA}$, $\alpha_1' C_{4\text{-CP}}$ and $\alpha_2' C_{BQ}$ in the denominator of Eq. 5, 6 and 7 were neglected because the values obtained were much lower than 1. Therefore, the final kinetic expressions employed for the parameters estimation were:

$$r_{CA}(\boldsymbol{x}, t) = (\alpha_{2,1} + \alpha_{2,2}) C_{CA}(\boldsymbol{x}, t)\left(-1 + \sqrt{1 + \frac{\alpha_1}{a_v} e^a(\boldsymbol{x})}\right) \quad (15)$$

$$r_{4\text{-CP}}(\boldsymbol{x}, t) = (\alpha_{4,1} + \alpha_{4,2}) C_{4\text{-CP}}(\boldsymbol{x}, t)\left(-1 + \sqrt{1 + \frac{\alpha_1}{a_v} e^a(\boldsymbol{x})}\right) \quad (16)$$

$$r_{BQ}(\boldsymbol{x}, t) = \alpha_5 C_{BQ}(\boldsymbol{x}, t)\left(-1 + \sqrt{1 + \frac{\alpha_1}{a_v} e^a(\boldsymbol{x})}\right) \quad (17)$$

Table 4 summarizes the estimated values of the kinetic parameters. $\alpha_{2,1}$ is the kinetic parameter involved in $r_{CA,1}$ and $\alpha_{2,2}$ is the parameter related with $r_{CA,2}$ (i.e. in the CA degradation to give the intermediate 4-CP and BQ, respectively). The value of $\alpha_{2,1}$ obtained with the optimization procedure was nearly ten times higher than $\alpha_{2,2}$. This result demonstrates that CA degradation via 4-CP is favored over the BQ pathway. On the other hand, the relatively high value of α_5 represents a significant rate of degradation of the BQ. Both results are in agreement with the low concentrations of BQ detected.

Figures 8 and 9 depicts the experimental concentrations of CA, 4-CP, and BQ and the concentrations estimated by the model under different operation conditions. The root mean square error (RMSE) of predictions was estimated according to: $\text{RMSE} = \left[\frac{1}{N}\sum_{i=1}^{N}\left(C_{i,\exp} - C_i/C_{i,\exp}\right)^2\right]^{1/2} \times 100$, where $C_{i,\exp}$ and C_i are the experimental and theoretical concentration of the species i, respectively. Also, N represents the total number of concentrations evaluated. The RMSE corresponding to the main pollutant was 5.9 %. Considering the three organic compounds, the RMSE was 16.6 %. Concentrations below 1×10^{-8} mol cm^{-3} are in the range of instrumental error so they were excluded from the calculations. It can be concluded that the model has a good capability to simulate the system behavior.

Conclusions

A kinetic model to represent the photocatalytic degradation of CA employing titanium dioxide in a slurry reactor has been developed. The values of the parameters involved in the kinetic expressions have been estimated by the optimizing procedure of Levenberg- Marquardt. The model accurately simulates the evolution of CA, 4-CP and BQ in a photocatalytic slurry reactor under different operation conditions (catalyst concentration and level of irradiation). The obtained kinetic parameters are independent of the irradiation conditions and reactor geometry, so this information could be useful for reactor designing or scaling-up purposes.

Appendix

Considering the competitive adsorption mechanism between CA and their principal intermediates, we can write the following equations:

$$[CA_{ads}] = K_{CA}[site_{CA}]C_{CA} \tag{18}$$

$$[4\text{-}CP_{ads}] = K_{4\text{-}CP}[site_{CA}]C_{4\text{-}CP} \tag{19}$$

$$[BQ_{ads}] = K_{BQ}[site_{CA}]C_{BQ} \tag{20}$$

$$[O_{2,ads}] = K_{O_2}[site_{O_2}]C_{O_2} \tag{21}$$

where $[j_{ads}]$ represents the concentration of the specie j adsorbed on the catalyst surface, K_j is the equilibrium adsorption constant, $[site_j]$ represents the superficial concentration of vacant adsorption sites, and C_j is the concentration of j in the suspension bulk.

Making a balance of sites we can relate the concentration of vacant sites to the total concentration of sites, $[site_{j,T}]$. Balance of absorption sites for O_2:

$$[site_{O_2,T}] = [site_{O_2,oc}] + [site_{O_2}] \tag{22}$$

where $[site_{O_2,oc}]$ represent the superficial concentration of occupied sites by O_2. Introducing Eq. (21) into Eq. (22):

$$[site_{O_2}] = \frac{[site_{O_2,T}]}{K_{O_2}C_{O_2} + 1} \tag{23}$$

Balance of absorption sites for the main organic compounds:

$$[site_{CA,T}] = [site_{CA,oc}] + [site_{CA}] \tag{24}$$

$$[site_{CA,T}] = [CA_{ads}] + [4\text{-}CP_{ads}] + [BQ_{ads}] + [site_{CA}] \tag{25}$$

Introducing Eq. (18)−(20) in Eq. (25):

$$[site_{CA}] = \frac{[site_{CA,T}]}{(K_{CA}C_{CA} + K_{4\text{-}CP}C_{4\text{-}CP} + K_{BQ}C_{BQ} + 1)} \tag{26}$$

Taking to account the assumption (v) made in the Kinetic model, the superficial degradation rate of i specie can be represented by:

$$r_i = k_i[\cdot OH][i_{ads}] \tag{27}$$

where k_i is the kinetic constant of the reaction between the organic compound and hydroxyl radicals, $[\cdot OH]$ is the concentration of hydroxyl radicals on the surface of the TiO_2 particles, and $[i_{ads}]$ represents the superficial concentration of i. Therefore, considering Eq. (27), the degradation pathway depicted in Fig. 3, and the reaction scheme presented in Table 3, the final degradation rate expressions for CA, 4-CP, and BQ are:

$$r_{CA} = k_5[\cdot OH][CA_{ads}] + k_6[\cdot OH][CA_{ads}] = (k_5 + k_6)[\cdot OH][CA_{ads}] \tag{28}$$

$$r_{4\text{-}CP} = k_7[\cdot OH][4\text{-}CP_{ads}] + k_8[\cdot OH][4\text{-}CP_{ads}] = (k_7 + k_8)[\cdot OH][4\text{-}CP_{ads}] \tag{29}$$

$$r_{BQ} = k_9[\cdot OH][BQ_{ads}] \tag{30}$$

Considering the superficial rate of appearance and disappearance of electrons, holes, and hydroxyl radicals shown in Table 3 and applying the kinetic micro-steady state approximation for the concentration of these species, the following expressions are obtained:

$$r_{e^-} = r_{gs} - k_2[e^-][h^+] - k_3[e^-][O_{2,ads}] \approx 0 \tag{31}$$

$$r_{h^+} = r_{gs} - k_4[h^+][H_2O_{ads}] - k_2[e^-][h^+] \approx 0 \tag{32}$$

$$r_{\cdot OH} = k_4[h^+][H_2O_{ads}] - (k_5 + k_6)[CA_{ads}][\cdot OH] - (k_7 + k_8)[4\text{-}CP_{ads}][\cdot OH] \\ - k_9[BQ_{ads}][\cdot OH] - \sum_l k_l''[\cdot OH][Y_{l,ads}] \approx 0 \tag{33}$$

where r_{e^-}, r_{h^+} and $r_{\cdot OH}$ correspond to the reaction rate of electrons, holes and hydroxyl radicals, respectively.

Operating with Eqs. (31–33) we obtain the expression for $[\cdot OH]$:

$$[\cdot OH] = \frac{k_3k_4[H_2O_{ads}][O_{2,ads}]\left\{-1 + \sqrt{\dfrac{1 + 4r_{gs}k_2}{k_3k_4[H_2O_{ads}][O_{2,ads}]}}\right\}}{2k_2\left\{(k_5 + k_6)[CA_{ads}] + (k_7 + k_8)[4\text{-}CP_{ads}] + k_9[BQ_{ads}] + \sum_l k_l''[Y_{l,ads}]\right\}} \tag{34}$$

Considering assumptions (vi), (vii) and (viii) of the kinetic model and introducing Eq. (34) into Eq. (28) we obtain:

$$r_{CA} = \frac{(\delta_{2,1} + \delta_{2,2})[CA_{ads}]\left\{-1 + \sqrt{1 + \delta_1 r_{gs}}\right\}}{\delta_3\left\{(k_5 + k_6)[CA_{ads}](k_7 + k_8)[4\text{-}CP_{ads}] + k_9[BQ_{ads}]\right\} + 1} \tag{35}$$

where

$$\delta_{2,1} = \frac{k_3k_4k_5[H_2O_{ads}][O_{2,ads}]}{2k_2\sum_l k_l''[Y_{l,ads}]} \qquad \delta_{2,2} = \frac{k_3k_4k_6[H_2O_{ads}][O_{2,ads}]}{2k_2\sum_l k_l''[Y_{l,ads}]}$$

$$\delta_1 = \frac{4k_2}{k_3k_4[H_2O_{ads}][O_{2,ads}]} \qquad \delta_3 = \frac{1}{\sum_l k_l''[Y_{l,ads}]}$$

Introducing Eq. (18–20) and Eq. (26) in Eq. (35):

$$r_{CA} = \frac{(\delta_{2,1} + \delta_{2,2})K_{CA}C_{CA}[\text{site}_{CA,T}]\{-1 + \sqrt{1 + \delta_1 r_{gs}}\}}{1 + \{[\text{site}_{CA,T}]\delta_3(k_5 + k_6)K_{CA} + K_{CA}\}C_{CA} + \{[\text{site}_{CA,T}]\delta_3(k_7 + k_8)K_{4-CP} + K_{4-CP}\}C_{4-CP} + \{[\text{site}_{CA,T}]\delta_3 k_9 K_{BQ} + K_{BQ}\}C_{BQ}}$$

Taking into account assumptions (ix) and (x) we obtain the kinetic expression that describes the rate of degradation of CA:

$$r_{CA}(\boldsymbol{x}, t) = \frac{(\alpha_{2,1} + \alpha_{2,2})C_{CA}(\boldsymbol{x}, t)}{1 + \alpha_3 C_{CA}(\boldsymbol{x}, t) + \alpha_1' C_{4-CP}(\boldsymbol{x}, t) + \alpha_2' C_{BQ}(\boldsymbol{x}, t)}$$

$$\left(-1 + \sqrt{1 + \frac{\alpha_1}{a_v} e^a(\boldsymbol{x}, t)}\right)$$

Where

$$\alpha_1 = \delta_1 \phi \qquad \alpha_{2,1} = \delta_{2,1} K_{CA}[\text{site}_{CA,T}]$$
$$\alpha_{2,1} = \delta_{2,1} K_{CA}[\text{site}_{CA,T}] \qquad \alpha_3 = \delta_3(k_5 + k_6)K_{CA}[\text{site}_{CA,T}] + K_{CA}$$
$$\alpha_1' = \delta_3(k_7 + k_8)K_{4-CP}[\text{site}_{CA,T}] + K_{4-CP} \quad \alpha_2' = \delta_3 k_9 K_{BQ}[\text{site}_{AC\ totals}] + K_{BQ}$$

Following the same procedure for 4-CP and BQ, reaction rates expressions were obtained for each of them:

$$r_{4-CP}(\boldsymbol{x}, t) = \frac{(\alpha_{4,1} + \alpha_{4,2})C_{4-CP}(\boldsymbol{x}, t)}{1 + \alpha_3 C_{CA}(\boldsymbol{x}, t) + \alpha_1' C_{4-CP}(\boldsymbol{x}, t) + \alpha_2' C_{BQ}(\boldsymbol{x}, t)}$$

$$\times \left(-1 + \sqrt{1 + \frac{\alpha_1}{a_v} e^a(\boldsymbol{x}, t)}\right)$$

$$r_{BQ}(\boldsymbol{x}, t) = \frac{\alpha_5 C_{BQ}(\boldsymbol{x}, t)}{1 + \alpha_3 C_{CA}(\boldsymbol{x}, t) + \alpha_1' C_{4-CP}(\boldsymbol{x}, t) + \alpha_2' C_{BQ}(\boldsymbol{x}, t)}$$

$$\times \left(-1 + \sqrt{1 + \frac{\alpha_1}{a_v} e^a(\boldsymbol{x}, t)}\right)$$

Where

$$\alpha_{4,1} = \frac{k_7 K_{4-CP} k_3 k_4 [H_2O_{ads}][O_{2,ads}][\text{site}_{CA,T}]}{2k_2 \sum_l k_l [Y_l]}$$

$$\alpha_{4,2} = \frac{k_8 K_{4-CP} k_3 k_4 [H_2O_{ads}][O_{2,ads}][\text{site}_{CA,T}]}{2k_2 \sum_l k_l [Y_l]}$$

$$\alpha_5 = \frac{k_9 K_{4-CP} k_3 k_4 [H_2O_{ads}][O_{2,ads}][\text{site}_{CA,T}]}{2k_2 \sum_l k_l [Y_l]}$$

References

Alfano OM, Cabrera MI, Cassano AE (1997) Photocatalytic reactions involving hydroxyl radical attack I. Reaction kinetics formulation with explicit photon absorption effects. J Catal 172:370–379

Almquist CB, Biswas P (2001) A mechanistic approach to modeling the effect of dissolved oxygen in photo-oxidation reactions on titanium dioxide in aqueous systems. Chem Eng Sci 56:3421–3430

Boyjoo Y, Ang M, Pareek V (2013) Light intensity distribution in multi-lamp photocatalytic reactors. Chem Eng Sci 93:11–21

Changrani R, Raupp GB (1999) Monte Carlo simulation of the radiation field in a reticulated foam photocatalytic reactor. AIChE J 45(5):1085–1094

De la Cruz N, Dantas R, Giménez J, Esplugas S (2013) Photolysis and TiO$_2$ photocatalysis of the pharmaceutical propranolol: solar and artificial light. Appl Catal B Environ 130–131:249–256

Dijkstra MFJ, Panneman HJ, Winkelman JGM (2002) Modeling the photocatalytic degradation of formic acid in a reactor with immobilized catalyst. Chem Eng Sci 57:4895–4907

Doll T, Frimmel F (2004) Kinetic study of photocatalytic degradation of carbamazepine, clofibric acid, iomeprol and iopromide assisted by different TiO$_2$ materials-determination of intermediates and reaction pathways. Water Res 38:955–964

Doll T, Frimmel F (2005) Photocatalytic degradation of carbamazepine, clofibric acid and iomeprol with P25 and Hombikat UV100 in the presence of natural organic matter (NOM) and other organic water constituents. Water Res 39:403–411

Dordio A, Estêvão Candeias A, Pinto A, Teixeira da Costa C, Palace Carvalho A (2009) Preliminary media screening for application in the removal of clofibric acid, carbamazepine and ibuprofen by SSF-constructed wetlands. Ecol Eng 35:290–302

Giraldo A, Peñuela G, Torres-Palma R, Pino N, Palominos R, Mansilla H (2010) Degradation of the antibiotic oxolinic acid by photocatalysis with TiO$_2$ in suspension. Water Res 44:5158–5167

Himmelblau DM (1970) Process analysis statistical methods. Wiley, New York

Imoberdorf G, Taghipour F, Keshmiri M, Mohseni M (2008) Predictive radiation field modeling for fluidized bed photocatalytic reactors. Chem Eng Sci 63:4228–4238

Martínez C, Canle M, Fernández M, Santaballa J, Faria J (2011) Kinetics and mechanism of aqueous degradation of carbamazepine by heterogeneous photocatalysis using nanocrystalline TiO$_2$, ZnO and multi-walled carbon nanotubes–anatase composites. Appl Catal B Environ 102:563–571

Mills A, Morris S, Davies R (1993) Photomineralisation of 4-chlorophenol sensitised by titanium dioxide: a study of the intermediates. J Photochem Photobiol A 70:183–191

Moreira J, Serrano B, Ortíz A, de Lasa H (2010) Evaluation of photon absorption in an aqueous TiO$_2$ slurry reactor using Monte Carlo simulations and macroscopic balance. Ind Eng Chem Res 49:10524–10534

Moreira J, Serrano B, Ortíz A, de Lasa H (2011) TiO2 absorption and scattering coefficients using Monte Carlo method and macroscopic balances in a photo-CREC unit. Chem Eng Sci 66:5813–5821

Murov SL, Carmichael I, Hug GL (1993) Handbook of photochemistry. Marcel Dekker, New York

Pelizzetti E, Minero C (1993) Electrochim Acta 38:47

Salgado R, Oehmen A, Carvalho G, Noronha J, Reis M (2012) Biodegradation of clofibric acid and identification of its metabolites. J Hazard Mater 241–242:182–189

Satuf ML, Brandi RJ, Cassano AE, Alfano OM (2005) Experimental method to evaluate the optical properties of aqueous titanium dioxide suspensions. Ind Eng Chem Res 44:6643–6649

Satuf ML, Brandi RJ, Cassano AE, Alfano OM (2007) Quantum efficiencies of 4-chlorophenol photocatalytic degradation and mineralization in a well-mixed slurry reactor. Ind Eng Chem Res 46:43–51

Siegel R, Howell JR (2002) Thermal radiation heat transfer. Hemisphere, Bristol, PA

Singh M, Salvadó-Estivill I, Li Puma G (2007) Radiation field optimization in photocatalytic monolith reactors for air treatment. AIChE J 53(3):678–686

Spadoni G, Bandini E, Santarelli F (1977) Scattering effects in photosensitized reactions. Chem Eng Sci 33:517–524

Terzian R, Serpone N, Minero C, Pelizzetti E, Hidaka H (1990) Kinetic studies in heterogeneous photocatalysis 4. The photomineralization of a hydroquinone and a catechol. J Photochem Photobiol A 55:243–249

Theurich J, Lindner M, Bahnemann DW (1996) Photocatalytic degradation of 4-chlorophenol in aerated aqueous titanium dioxide suspensions: a kinetic and mechanistic study. Langmuir 12:6368–6376

Turchi CS, Ollis DF (1990) Photocatalytic degradation of organic water contaminants: mechanisms involving hydroxyl radical attack. J Catal 122:178–190

Wu Q, Shi H, Adams C, Timmons T, Ma Y (2012) Oxidative removal of selected endocrine-disruptors and pharmaceuticals in drinking water treatment systems, and identification of degradation products of triclosan. Sci Total Environ 439:18–25

Yokota T, Cesur S, Suzuki H, Baba H, Takahata Y (1999) Anisotropic scattering model for the estimation of light absorption rates in photoreactor with heterogeneous medium. J Chem Eng Jpn 32:314–321

Zazueta A, Destaillats H, Li Puma G (2013) Radiation field modeling and optimization of a compact and modular multi-plate photocatalytic reactor (MPPR) for air/water purification by Monte Carlo method. Chem Eng J 217:475–485

Zekri M, Colbeau-Justin C (2013) A mathematical model to describe the photocatalytic reality: what is the probability that a photon does its job? Chem Eng J 225:547–557